



## Josephson Effect in MgB<sub>2</sub>/Pd/Nb Trilayer Josephson Junctions

Anayesu B Malisa

Department of Physics, College of Natural and Applied Sciences, University of Dar es Salaam, P.O. Box 35063, Dar es Salaam, Tanzania

E-mail: [amalisa@udsm.ac.tz](mailto:amalisa@udsm.ac.tz)

Received 25 Jan 2021, Revised 10 July 2021, Accepted 20 Jul 2021, Published Aug 2021

DOI: <https://dx.doi.org/10.4314/tjs.v47i3.17>

### Abstract

This paper reports fabrication techniques and results of MgB<sub>2</sub>/Pd/Nb trilayer Josephson junctions. The MgB<sub>2</sub> bottom electrode was co-evaporated by molecular beam epitaxy (MBE) technique from both magnesium and boron sources at a low substrate temperature ~ 300 °C, while the interlayer and the top niobium electrode (Pd/Nb bilayer) were deposited *ex-situ* using RF sputtering. The junctions exhibited *dc* and *ac* Josephson effect as well as a modulation of the critical current in a magnetic field applied in a direction normal to the junction plane. Fractional and integer Shapiro steps were observed at voltages corresponding to the frequency of the applied microwave radiation field. The  $I_c R_N$  products of the junctions compare well with the previously reported values. The results suggest that it should be possible to fabricate all-MgB<sub>2</sub> and MgB<sub>2</sub> as one of the electrodes Superconductor/Normal/Superconductor (SNS), Superconductor/Insulator/Superconductor (SIS) or even Superconductor/Ferromagnet/Superconductor (SFS) tunnel junctions with interesting characteristics and for various applications.

**Keywords:** MgB<sub>2</sub>, all-MgB<sub>2</sub>, Josephson Tunnel junctions, trilayer devices, Niobium.

### Introduction

The discovery of superconductivity in magnesium diboride (MgB<sub>2</sub>) at 39 K (Nagamatsu et al. 2001) brought a lot of enthusiasm to the superconductivity research community. Since its discovery, considerable development in the areas of thin film preparation (Xi et al. 2004) and device fabrication based on this superconductor have been achieved. The present focus is, to a large extent, directed towards the choice of suitable interlayer or barrier materials and how to fabricate MgB<sub>2</sub>/interlayer/MgB<sub>2</sub> or MgB<sub>2</sub>/barrier/MgB<sub>2</sub> trilayer devices. All-MgB<sub>2</sub> multilayer junctions made in a ramp type (Mijatovic et al. 2002, Mijatovic et al. 2003) and step-edge (Kye et al. 2003) configurations have been realized. Tunnel junctions using as-grown MgB<sub>2</sub> thin films, AlN as a barrier and

NbN counter-electrode have been reported (Saito et al. 2002). Moreover, tunnel junctions fabricated on as-grown MgB<sub>2</sub> thin films with MgO<sub>x</sub> or AlO<sub>x</sub> (Shim et al. 2007) barriers and *in-situ* deposited normal metal Au, Ag or superconducting MgB<sub>2</sub> thin film counter-electrodes have also been reported (Ueda and Naito 2003a, Ueda and Naito 2004, Chen et al. 2008). Planar MgB<sub>2</sub> Josephson junctions fabricated via nanolithography and ion damage exhibiting interesting and useful practical properties have also been reported (Cybart et al. 2006).

This paper reports fabrication techniques and results of MgB<sub>2</sub>/Pd/Nb trilayer Josephson junctions. These junctions were found to exhibit both *dc* and *ac* Josephson effects first explained by B. D. Josephson (Josephson 1962) and by many others after him including

recently (Schmid and Menke 2015). A Josephson junction describes a weak link between two superconductors. The weak link as we have already seen can for instance be a normal metal, N, an insulator, I, a ferromagnetic material, F, etc. In 1962, B. D. Josephson made two predictions, and these are; a supercurrent,  $I_s$ , would evolve between two superconducting electrodes as  $I_s = I_c \sin(\varphi)$ , with  $I_c$  describing the critical or switching current, which designates the maximum supercurrent the junction can support, that is  $I_c = \max[I_s(\varphi)]$ , and  $\varphi$  the phase difference of the condensate wave functions of the Ginzburg-Landau theory. This phenomenon is known as the *dc* Josephson effect. It was later verified experimentally that this showed even in the absence of a potential drop there may be a supercurrent which depends on the phase difference across the junction. It should be understood that this simple current-phase relation (CPR) is only valid in the limit of one or multiple channels with low transparency. The other prediction was that if a voltage,  $V$ , is applied across the junction the phase difference  $\varphi$ , evolves as follows,  $\frac{d\varphi}{dt} = \frac{2eV}{\hbar}$ , where  $\hbar$  is the reduced Planck's constant and  $e$  is the elementary charge. This corresponds to an oscillating supercurrent with frequency  $\nu_j = \frac{2eV}{h}$ , with  $\nu_j$  describing the Josephson frequency and  $h$  the Planck's constant and it is known as the *ac* Josephson Effect. This phenomenon has also been verified experimentally and is the basis for Josephson junctions' applications in the terahertz frequency range. The quantity  $\frac{h}{2e}$  in the second Josephson relation  $\varphi(t) = \frac{2e}{\hbar} Vt$  or  $\frac{d\varphi}{dt} = \frac{2eV}{\hbar}$  is a magnetic flux quantum  $\Phi_0 \sim 2.07 \times 10^{-15}$  Webers (Wb) or volt – second (Vs) or  $\frac{V}{\text{Hz}}$ . Note also that:  $1 \text{ Wb} = 1 \text{ Tm}^2$  (Tesla-metre squared). The smallness of the magnetic flux quantum ( $\Phi_0^{-1} = \frac{2e}{h} \sim 0.483 \frac{\text{GHz}}{\mu\text{V}}$ ) shows that a small variation of the voltage drop  $V$  over a junction leads to a fast variation of the phase difference  $\varphi(t)$

between the two superconducting electrodes. Application of the Josephson effect is in metrology (especially as a standard volt) through the relation,  $V = \frac{h}{2e} \nu = \Phi_0 \nu$ . For example this can give us a precise definition of electrical voltage by using fundamental constants at a high precision largely uninfluenced by environmental parameters at any place in the world. Also precise measurements of the electron charge is made from the Josephson constant  $\frac{h}{2e}$  and the von Klitzing constant  $\frac{h}{e^2}$  measured in the quantum Hall effect. Josephson junctions are very versatile non-linear circuit elements which can also find applications as highly accurate magnetometers and radiation detectors. The tunnelling SIS Josephson junctions in particular can be used as superconducting quantum bits or qubits for building quantum computers (Tsai 2010, Mohseni et al. 2017).

When presenting Josephson junctions' properties it is standard to include two experiments: magnetic field,  $B$ , dependence of the critical current,  $I_c$ , that is  $I_c(B)$  and microwave field irradiation. In the first experiment the magnetic field modulated critical current gives a maximal Josephson current and its modulus is similar to the refraction on a single slit called a Fraunhofer pattern. The second experiment results in the appearance of constant voltage plateaus, called Shapiro steps (Shapiro 1963) in the current-voltage ( $I - V$ ) characteristics of the junctions. This is because when a Josephson junction is irradiated with microwave radiation field of frequency, it has the ability to be in a resonance or phase-locked to the field and this manifests itself as Shapiro steps in the  $I - V$  curves. With typical microwave excitation frequencies  $\nu > 1 \text{ GHz}$ , it is possible to observe measurable Shapiro steps. These experiments verify that the junctions are truly exhibiting the two Josephson effects. The magnetic field dependence of the critical current is a verification of the *dc* Josephson relation, while

the presence of Shapiro steps confirm the *ac* Josephson relation.

However, it has been found that in some Josephson junctions with non-sinusoidal CPRs, substeps or subharmonic steps can also occur at voltages  $V_{n/m} = (n/m)(h/2e)v$ , with  $n = 0, \pm 1, \pm 2, \dots$  and  $m = 1, 2, 3, \dots$ ;  $m$  is the order of the steps and  $n \neq m$ . These fractional Shapiro steps, including the famous half-integer Shapiro steps and other fractional ones, all have their origin from the phase-locked response with the  $m^{\text{th}}$  harmonic in the CPR of the Josephson junction. Sinusoidal CPRs have  $2\pi$  periodic phases while non-sinusoidal ones have periodicity different from  $2\pi$ .

Fractional Shapiro steps can also be attributed to synchronization of the motion of Josephson vortices along the junction with the microwave radiation field. However, it is impossible for Josephson vortices to enter, be captured or flow in junctions in which the Josephson penetration length is larger than the junction dimension.

## Materials and Methods

### Junction fabrication

MgB<sub>2</sub> films used as base electrodes in the junctions were deposited by molecular beam epitaxy (MBE) technique on Al<sub>2</sub>O<sub>3</sub> (0001) substrates. Details of how the MgB<sub>2</sub> films were deposited and their characterizations are similar to those described in Ueda and Naito (2001), Ueda et al. (2002), and Ueda and Naito (2003b). A bilayer of Pd/Nb film was deposited by RF sputtering. First the MgB<sub>2</sub> film surface was cleaned by a sputtering process at low RF power. Then a 10 – 15 nm thin film of Pd was sputtered onto the MgB<sub>2</sub> film surface followed by an *in-situ* sputter of a 200 nm in thickness of superconducting Nb film in a Sputter-Pfeiffer system Model SLS-630G 'Spider' (Pfeiffer Vacuum, Germany).

The junctions' patterns and alignment marks transfer from the photomask onto the multilayered film surface followed standard photolithography steps commonly used in nano- and micro-fabrication of electronic devices. In the first step, the process started by

spin coating a photoresist (a light-sensitive polymer) on a clean multilayered film sample surface using a spinner. A positive photoresist Shipley 1813 (S-1813) was coated on the multilayered film in this case MgB<sub>2</sub>/Pd/Nb at 6000 rpm (revolution per minute) and for 1 minute to give about 500 nm in thickness of the resist. In the second step, the resist film was pre-baked or soft-baked on a hotplate at a temperature of 95 °C and for 2 minutes to remove solvents. The third step involved photomasks alignment in a mask aligner. The photomasks were produced by an electron beam lithography (EBL) of a chromium metal film deposited on a quartz surface in a process called maskless lithography using EBL system - JEOL JBX 9300FS (JEOL Ltd., Japan).

A photomask with the needed patterns/structures and alignment marks was accurately aligned and brought into contact with the sample surface already coated with photoresist in a Karl SUSS MJB3 Mask Aligner/Exposure System (Karl SUSS, Germany). The equipment was equipped with a lamp of which its radiation wavelength and intensity were 400 nm and 6 mW/sqcm, respectively. The fourth and fifth steps involved selective ultraviolet (UV) light exposure of the photoresist film through a frame photomask pattern for 45 seconds and developing in a developer microfabrication (MF) 322 solvent for 20 seconds, respectively. During exposure, the shadow casted by the mask frame/structure was transferred to the sample surface. The UV light changed the chemical structure of the photoresist to make it soluble in the developer solvent. Then the sample was rinsed in de-ionized (DI) water to remove the exposed photoresist and also to prevent overdeveloping. This procedure was repeated when every similar lithography stage was completed. A sharp frame pattern was revealed on the sample surface when examined with an optical microscope. Another mask alignment and photoresist exposure through the structures or MgB<sub>2</sub> loop photomask was done. The exposure and developing time for the

structures or MgB<sub>2</sub> base electrodes were 10 and 5 seconds, respectively.

The fine structures/patterns of MgB<sub>2</sub> bottom electrodes were clearly revealed in the remaining unexposed photoresist on the sample surface. The unexposed photoresist acted as an etch mask during etch processes.

Two types of dry etching processes: reactive ion etching (RIE) and ion beam etching/milling (IBE) were used. First, to obtain the MgB<sub>2</sub> base electrodes RIE of the Nb layer in a carbon tetrafluoride (CF<sub>4</sub>) plasma at 100 mTorr was done in a Plasma Therm BatchTop equipment. This etch process was completed by Argon-ion beam milling of the Pd and MgB<sub>2</sub> layers in a chemically assisted ion beam etching (CAIBE) system - Oxford Ionfab 300 equipment. After stripping the photoresist in acetone and isopropanol (IPA) another photolithography and RIE of the Nb layer processes were carried out to pattern the junction areas as follows. A 100 nm silicon dioxide (SiO<sub>2</sub>) thin film was deposited by e-beam evaporation technique to provide electrical insulation for the junctions and windows for Nb wiring layer. The unwanted layer of SiO<sub>2</sub> dielectric was removed through photolithography and lift-off processes. A Nb contact and wiring layer, 200 nm in thickness was then deposited and patterned using photolithography and etching by RIE processes as before. Finally, gold contact pads were deposited through a lift-off stencil consisting of two layers of photoresists; the lift-off layer 2000 (LOL-2000) or spacer layer and S-1813. The LOL-2000 resist was first spin coated on the sample at 3000 rpm for 1 minute and baked at 130 °C for 5 minutes followed by S-1813 resist which was spin coated at 4000 rpm for 1 minute and baked at 110 °C for 2 minutes. The LOL-2000 resist layer was used to ensure that we obtained an undercut required for a good lift-off of the unwanted photoresists and gold film layers. A titanium underlayer film between 5 to 10 nm in thickness was first deposited before depositing the gold film to obtain a good adhesion of the gold film for the contacts pads. Both the

titanium underlayer film and the gold film for the contact pads were deposited using e-beam evaporation technique in e-beam evaporator (AVAC HVC600 system). The thickness of the gold contact pads layer was 180 nm. A lift-off of the photoresists and gold layer on chip areas where these were not needed and a final photoresists cleaning was done in acetone.

The sizes of the fabricated junctions were 10 × 10, 20 × 20 and 30 × 30 μm<sup>2</sup>, the largest junctions on the chip being 30 × 30 μm<sup>2</sup> and the smallest 10 × 10 μm<sup>2</sup>. Figure 1 is an optical micrograph (captured using Optical Microscope - Olympus MX50 ) to depict parts of the chip on which the junctions are fabricated. Two of the junctions in the micrograph can clearly be seen to be of different sizes. Figure 2 is a scanning electron microscope (SEM) micrograph obtained by SEM-JEOL JSM 6301F (JEOL Ltd., Japan) of part of the chip showing one of the junctions fabricated.

#### **Junction electrical, microwave and magnetic field characterization**

Measurement setup consisted of a resistor box (custom designed) for current or voltage biasing circuit of a junction's electrical transport measurement. It also consisted of two pre-amplifiers (Princeton Applied Research Pre-Amp model 5113) for amplifying a junction current and voltage signals (increasing their signal-to-noise ratios) during  $I - V$  curve measurement. There were also batteries for powering the pre-amplifiers, and also a liquid helium-4 ( $He^4$ ) dewar for dipstick (custom-designed) insert during sample cooling and measurements. All these were kept inside of an electrical or radiofrequency (RF) noise shielded room to reduce external electrical noise from nearby motors, transmitters, mobile phones, etc. Stationed outside the shielded room was a voltage source (Agilent 33220A 20 MHz Function/Arbitrary Waveform Generator) used to generate a low frequency triangular voltage signal,  $V_{bias}$ , for biasing a junction during  $I - V$  measurement. In addition to that there were two multimeters (HP 34401A

Multimeters) for measuring junction current and voltage signals, an oscilloscope (Fluke PM 3380A–Autoranging Combiscope 100 MHz) for junction current and voltage signals display, a temperature controller (Conductus LTC) and a personal computer (PC) running a LabVIEW program. All signals from the multimeters, voltage source and temperature controller were connected to the PC via a data acquisition (GPIB interface) card. The temperature controller was used to operate, via the PC and the LabVIEW software, a temperature sensor and heater on the dipstick, mounted at right locations to provide necessary thermal contacts to the sample holder and its sample. Also placed outside the shielded room were *dc* current source (Yukogawa 7651 Programmable DC source), which was used to supply *dc* electrical current to a solenoid with a calibrated field rate and a microwave source (Anritsu 68377C Synthesized Signal Generator - 100 MHz to 50 GHz) connected to a microwave antenna. Magnetic fields produced by the solenoid and the microwave radiation fields from the antenna were used in the magnetic field,  $B$ , dependence of the junctions' critical current,  $I_c$ , that is  $I_c(B)$  and junctions' microwave irradiation experiments, respectively. A coaxial and fiber-optic cable connected the current and microwave source, respectively, to capacitive filters on the outside wall of the shielded room. From the inside wall of the room and onto the dipstick in the room, coaxial cables were used for both connections. All measurement lines running along the dipstick to the sample were inductively filtered. Amplified signals from the pre-amplifiers were transmitted in coaxial cables to measurement instruments outside the shielded room through feed-through filters on the wall of the room.

External stray magnetic fields shielding, however, was provided by a  $\mu$ -metal shield around both sample holder and sample on the dipstick. Additional magnetic shielding was provided by a superconducting shield fitted

inside the liquid helium dewar to shield the dipstick and sample.

The junctions were patterned for a four-point electrical measurements configuration and were wired to a sample/chip carrier using a wire bonder machine. The chip carrier with its sample was then placed in its position on the dipstick. The dipstick was enclosed in a cylindrical metal case and all connections to various measurement instruments were made via BNC connectors on the other end of the dipstick.

Connections between the chip carrier leads and the dipstick were done in such a manner that any junction on the chip could be chosen for measurements with no need for withdrawing the dipstick from the helium dewar.

For the current-biased measurements a large bias resistor ( $R_{bias} \sim 1 M\Omega$ ) was connected in series with the junction in order to generate a (small) bias current flowing through the junction. The junction was set in parallel with a small shunt resistor ( $R_s \sim 3 - 10 \Omega$ ) and hard-ground was provided by the chip carrier grounding leads. A junction's temperature dependence of resistance measurement was performed while the dipstick was cooled from room temperature ( $\sim 300 K$ ) down to temperatures well below the critical temperatures of MgB<sub>2</sub> (39 K) and Nb (9.3 K) in the liquid helium dewar. The helium dewar had a base temperature of 4.2 K (boiling temperature of liquid helium), the temperature at which many of the electrical transport measurements were performed. Withdrawal of the dipstick from the liquid helium to the helium gas above it, while still in the dewar and in combination with the heater to slightly warm the sample (when necessary) it was possible to perform measurements at any other temperature above 4.2 K. All measurements were done with the help of the LabVIEW program.

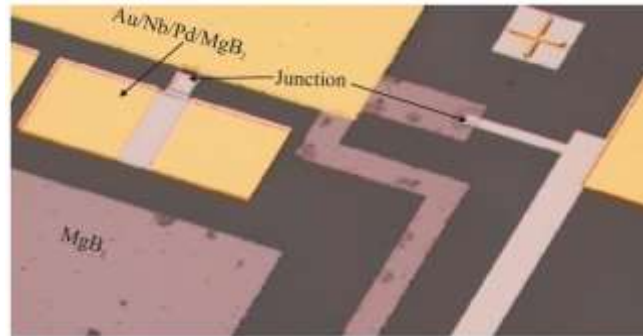


**Figure 1:** An optical micrograph of part of the chip depicting two sizes of junction devices. Note that the cross seen in the micrograph is one of the alignment marks.



**Figure 2:** An SEM micrograph of one of the MgB<sub>2</sub>/Pd/Nb trilayer junctions fabricated.

### Results and Discussion

The results presented and discussed here are mainly from junctions with junction size of  $30 \times 30 \mu\text{m}^2$  because of their interesting  $I - V$  characteristics. Electrical measurements performed on junctions of the other sizes show similar results but with less critical currents. The temperature dependence of resistance,  $R(T)$ , of one of the junctions shows critical temperature of Nb at  $T_{cNb} \sim 9.2 \text{ K}$  and that of MgB<sub>2</sub> at  $T_{cMgB_2} \sim 31 \text{ K}$  (Figure 3).

The current-voltage ( $I - V$ ) characteristics of the junctions were measured at 4.2 K (Figure 4) and from 4.8 K up to 7.4 K as well as from 4.2 K up to 12.5 K as shown in Figure 5. The inset to Figure 5 (upper panel) is the temperature dependence of the critical current,  $I_c(T)$ . Above  $T_{cNb}$  there was no supercurrent observed in the junction. The temperature dependence of the critical current over all temperature range below  $T_{cNb}$ , can be approximated by the expression  $(1 - T/T_{cNb})^\alpha$ , where  $\alpha$  in this case will take the

value of 1 for temperatures well below  $T_{cNb}$  and 2 for temperatures close to  $T_{cNb}$ .

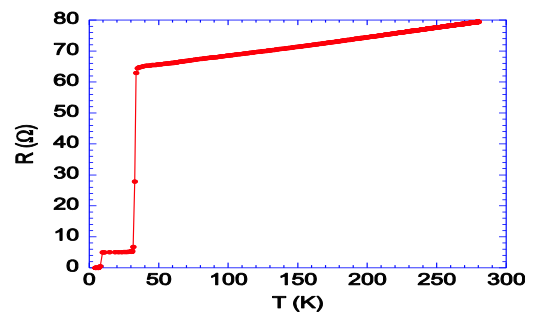


**Figure 3:** Temperature dependence of resistance of an MgB<sub>2</sub>/Pd/Nb Josephson junction. The critical temperature of MgB<sub>2</sub> base electrode is  $\sim 31 \text{ K}$  and that of Nb top electrode is  $\sim 9.2 \text{ K}$ .

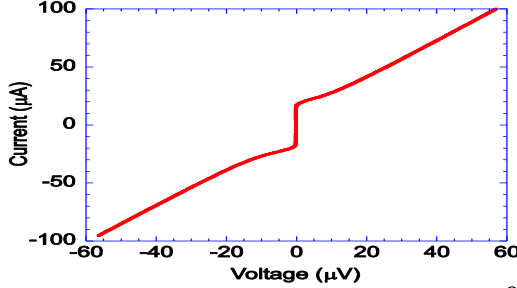


**Figure 4:** An  $I - V$  curve of a  $30 \times 30 \mu m^2$  junction measured at  $4.2 K$  and a  $2.5 \mu T$  magnetic field applied in the direction normal to the junction plane. The value of the critical current is suppressed by the magnetic field.

Shapiro steps were observed at voltage values corresponding to the Josephson relation  $V_n = nhv / 2e$ , where  $v$  is the frequency of the applied microwave radiation field,  $h$  is the Planck's constant,  $e$  is elementary charge and  $n$  is an integer. When the junction with the  $I - V$  curve in Figure 4 was irradiated with a microwave radiation field of frequency  $5.799 GHz$  and a magnetic field of  $2.5 \mu T$  applied in a direction normal to the junction plane, Shapiro steps occurred at multiples of voltage value of  $12 \mu V$  as shown in Figure 6. The  $I - V$  curves are plotted at different microwave power levels ranging from  $P = -11.9 dBm$  to  $P = +4 dBm$ .

Half-integer multiples of integer or normal Shapiro steps at voltage steps of  $\sim 6.7 \mu V$  along with the Shapiro steps at voltage steps of  $13.4 \mu V$  corresponding to the frequency of the microwave radiation field applied were observed in another junction when irradiated with microwave field of frequency  $6.941 GHz$  and a magnetic field of  $125 \mu T$  (Figure 7 (upper panel)). The applied magnetic field was in a direction normal to the junction plane. In addition to the conventional integer and half-integer Shapiro steps at  $V \approx 6.7 \mu V$ , additional  $1/3$  and  $2/3$  fractions of the normal Shapiro steps were also observed (Figure 7 (upper panel)). The half-integer Shapiro steps could have appeared due to the existence of the second harmonic in the junction's CPR. They could also be related to the period doubling

under the large microwave signal at frequency not far from plasma frequency  $\nu_p = \nu_c(\beta_c)^{-1/2}$  of the Josephson junction, where  $\nu_c = (2e/h)I_cR_N$  is the characteristic or critical frequency and  $\beta_c = (2e/h)I_cR_N^2C$ , is the Stewart - McCumber parameter. The fractional Shapiro steps depicted in Figure 7 (upper panel) are not only intrinsic to the junctions but are also due to the applied magnetic field. This is because the fractional Shapiro steps were not well pronounced or observed when the junction was irradiated with microwave radiation of frequency  $11.7315 GHz$  and  $11.7325 GHz$  at power  $P = +12.98 dBm$  and  $P = +13.22 dBm$ , respectively, but without applying magnetic field (See Figure 7 (lower panel)) or when the magnetic field was too small, for example  $2.5 \mu T$  in Figure 6.

The Josephson penetration depth,  $\lambda_j$ , for the junction was obtained from the expression  $\lambda_j = \sqrt{\frac{\Phi_0}{4\pi\mu_0dJ_c}}$ , with  $\Phi_0$  as a magnetic flux quantum,  $J_c = 5.6 \times 10^4 Am^{-2}$  as the junction's critical current density,  $d \sim \lambda_{L(MgB_2)} + \lambda_{L(Nb)} + t$ , where  $\lambda_L$  is the London's penetration depth and  $t$  is the junction's barrier thickness and  $\mu_0 = 4\pi \times 10^{-7} Wb/(A.m)$ , that is the permeability of free space. Using London's penetration depths  $\lambda_{L(MgB_2)} = 185 nm$  and  $\lambda_{L(Nb)} = 43 nm$ , the junction's barrier thickness  $t \sim 15 nm$  and the other parameters in the relation to determine  $\lambda_j$  gives  $\lambda_j \sim 98.1 \mu m$ , a value which is larger than the junction dimension  $w = 30 \mu m$ . It is understood that Josephson vortices cannot enter the junction area and be captured by the junction or flow in the junction since the junction dimension is smaller than the Josephson penetration length, as  $w < \lambda_j$ , so the junction is in the short junction limit and can be taken as a point object whose dynamics are described by the resistively shunted junction (RSJ) model.

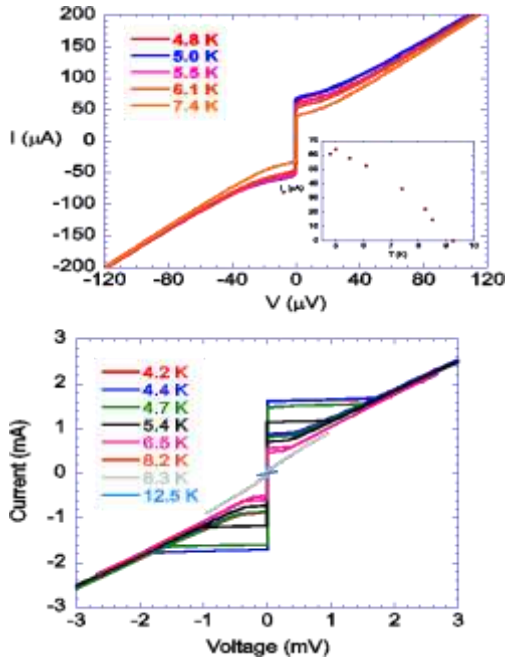


**Figure 5:**  $I - V$  curves of a  $30 \times 30 \mu\text{m}^2$  junction measured from 4.8 K to 7.4 K. The inset is a plot of temperature dependence of critical current of the junction (upper panel).  $I - V$  curves of another junction measured from 4.2 K to 12.5 K (lower panel).

Modulation of the critical current by an externally applied magnetic field was studied by applying a magnetic field in a direction normal to the junction plane. The magnetic coil used could only give a magnetic field in this direction but it could be that there was a component of the field in the plane of the junctions. Shown in Figure 8 is the modulation of the critical current of the junction with the  $I - V$  curve depicted in Figure 4. The magnetic field dependence of the critical current,  $I_c(B)$ , pattern of the junction shown in Figure 8 was observed when the magnetic field was applied in a direction normal to the junction plane.

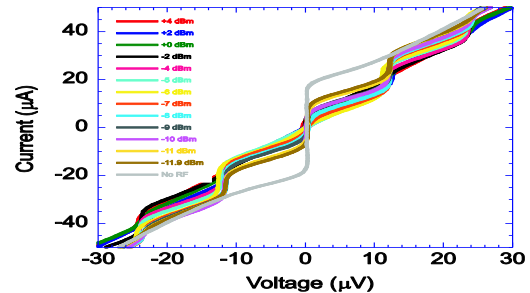


**Figure 6:** An  $I - V$  curve of a junction with  $2.5 \mu\text{T}$  magnetic field applied in a direction normal to the junction plane and irradiated with microwave radiation field of frequency  $\nu = 5.799 \text{ GHz}$  at different power levels. Shapiro steps appear at voltages equal to integral multiples of  $\Phi_0\nu = 12 \mu\text{V}$  ( $\Phi_0 = h/2e$ ).

The observed  $I_c(B)$  diffraction pattern is not the ideal Fraunhofer pattern. This might be due to a non-homogeneous field in the plane of the junction because of the direction the magnetic field was applied which was not in the plane of the junction. Another reason could be a non-homogeneous current distribution in the junction due to the presence of pinholes. However, an  $I_c(B)$  pattern similar to the one shown in Figure 8 can be observed even in junctions with homogeneous interfaces if a magnetic field applied normal to the junction plane has only a small component in the plane of the junction. Moreover, the smooth surface morphology of the  $\text{MgB}_2$  films used and the thickness of the Pd interlayer film of  $10 - 15 \text{ nm}$  which was smooth and continuous could indicate that the interfaces were homogeneous.

The trilayer  $\text{MgB}_2/\text{Pd}/\text{Nb}$  junctions fabricated suggested that there are prospects of realizing all- $\text{MgB}_2$  or  $\text{MgB}_2$  as one of the electrodes with another superconductor as a second electrode based Josephson junctions with junction properties suitable for various applications. The critical current and normal resistance products,  $(I_c R_N)$  products, also called characteristic voltage,  $V_c$ , of the junctions with  $I - V$  curves depicted in Figure 5 at 4.8 K and 4.2 K are  $50 \mu\text{V}$  (upper panel) and  $2.7 \text{ mV}$  (lower panel). The  $I_c R_N$  product of

a Josephson junction is a common figure-of-merit for determining the operating speed of the Josephson junction. Figure 5 (lower panel) shows that the  $I - V$  curve of the junction is hysteretic due to possibly junction's capacitance. The value of the critical current,  $I_c$  and retrapping or reset current,  $I_r$  are  $1.7 \text{ mA}$  and  $0.9 \text{ mA}$ , respectively. The area of this junction is  $30 \times 30 \mu\text{m}^2$  and so its critical current density  $J_c \approx 2 \times 10^2 \text{ Acm}^{-2}$ . The ratio between retrapping current and critical current,  $I_r/I_c$  defines the hysteresis ratio for a junction which was  $0.53$  for this junction. The Stewart-McCumber parameter,  $\beta_c$ , value of this junction, as deduced from the relation  $\beta_c = (4I_c/\pi I_r)^2$  is approximately equal to  $6$ . The  $I - V$  characteristics of the junction in the upper panel of Figure 5 can be explained by the simple RSJ model. That is, below the critical current,  $I_c$ , the junction is carrying a non-dissipative supercurrent at a zero voltage. As the bias current exceeds the critical,  $I_c$ , the junction abruptly jumps to a resistive state. The extra current is carried by a resistive channel of quasiparticle excitations and so a non-zero voltage appears across the junction and the  $I - V$  relationship becomes ohmic. If the bias current is decreased from  $(I_{bias})$ ,  $I > I_c$ , the junction returns to the superconducting state only at a current  $I_c$ , since it is in the overdamped regime ( $\beta_c \ll 1$ , *small C*). The  $I - V$  characteristics of the junction in the lower panel, however, can be explained by the resistively and capacitively shunted junction (RSCJ) model. In this, we see the junction returns at a current,  $I_r$ , lower than the critical or switching current,  $I_c$ , and so it is in the intermediate damped or underdamped regime ( $\beta_c \gg 1$ , *large C*). It may also be argued that the hysteretic behaviour in the junction's  $I - V$  characteristics may be due to heating effects and this argument can be supported by the junction's large amount of the critical current of  $1.7 \text{ mA}$ .

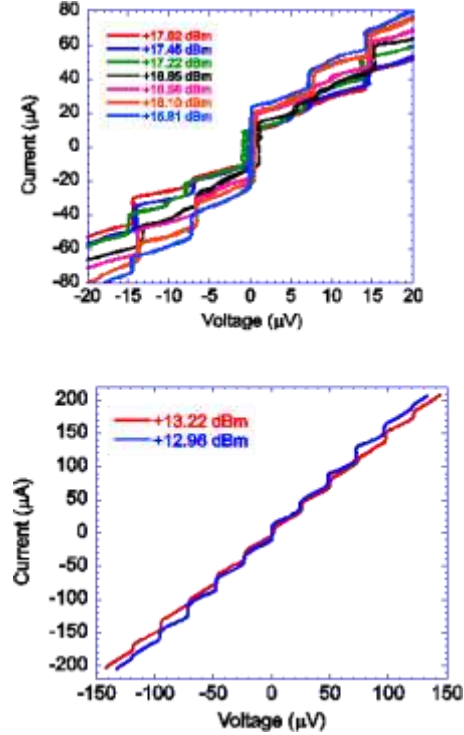


**Figure 7:** Shapiro steps at integer multiples of the voltage  $13.4 \mu\text{V}$ , half-integer as well as  $1/3$  and  $2/3$  of normal Shapiro steps observed in a junction's  $I - V$  characteristics when irradiated with a microwave radiation field of frequency  $6.941 \text{ GHz}$  at different microwave power levels and a magnetic field of  $125 \mu\text{T}$  applied (upper panel). The same junction when irradiated with a microwave field of frequency  $11.7315 \text{ GHz}$  and  $11.7325 \text{ GHz}$ , respectively, and at different microwave power levels. Fractional Shapiro steps were not clearly observed with no magnetic field applied (lower panel).

As Pd is used to make good electrical contacts we can argue that using Pd as an interlayer material in SNS junctions can give a homogeneous interface with high interface transparency of approximately unity. This can be the case especially when there are no interface imperfections due to surface roughness of the first layer. However, the effects of Pd as a highly paramagnetic metal on the Nb and MgB<sub>2</sub> superconductors or the

quality of the interface have not been investigated. If a superconductor forms an interface with a magnetic metal the following effects can take place. The effects are the spin sub-bands splitting and spin-dependent impurity scattering. The transparency of the interface is affected due to one or both of these reasons combined. Other reasons which can affect interface transparency are intrinsic reasons like the difference in Fermi velocities of the electrons in the normal metal and the superconductor as well as their electronic band structures. These effects make electrons incident at the interfaces to be reflected rather than transmitted hence screening the proximity effect.

The  $I - V$  measurements performed up to the gap voltages of the two superconductors, Nb and MgB<sub>2</sub> did not show energy gap structures of either Nb or MgB<sub>2</sub> superconductors. Pd, like Au and Ag, has a zero or negative interaction potential  $U$ . At the Nb or MgB<sub>2</sub> interface the Nb or MgB<sub>2</sub> electron pair amplitude, denoted here by  $F$ , will decay into Pd if there is not additional breaking of Cooper pairs due to the nearly magnetic Pd metal. The electron pair potential  $\Delta = F.U$  will therefore be zero (or negative). The quasiparticles of all energies from the superconductors will be allowed in Pd but there is no strict energy gap. That is there are no energies for which the density of states is zero. However, if ballistic transport occurs we may observe energy gap structures in a metal with the interaction potential  $U = 0$ . This is not because the states in the normal metal are forbidden but simply because fewer electrons of this energy and more electrons of energy  $E \approx \Delta$  enter the normal metal layer from the superconductor.

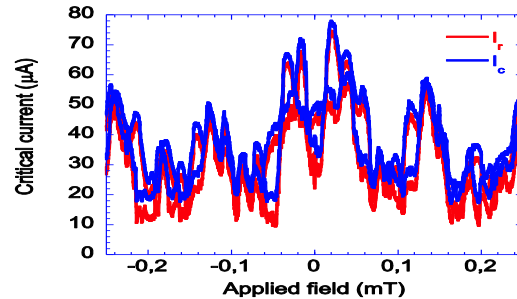


**Figure 8:** Critical current dependence of the magnetic field. The magnetic field diffraction pattern of the critical current observed here is not the ideal Fraunhofer pattern.  $I_c$  and  $I_r$  are the critical current and retrapping or return current of the junction, respectively.

For this effect to be observed, it is important for the normal metal layer not be dirty or too thick. Since energy gap structures were not observed in the junctions'  $I - V$  characteristics and the thickness of the Pd interlayer was thin (Pd interlayer film thickness was only between 10 – 15 nm), it can be argued that the absence of energy gap structures is due to dirty Pd interlayer film. Transition metals like Pd have Fermi velocities  $v_F \sim (1 - 2) \times 10^6 \text{ ms}^{-1}$ . The normal coherence or decay lengths  $\xi_{nc}$  at 4.2 K corresponding to these Fermi velocities are  $\xi_{nc} = 300 - 600 \text{ nm}$  (Kye et al. 2003, Delin and Kleinsasser 1996). In thin films normal electron mean free paths,  $\ell_n$ , are limited by film thickness. The electron mean free path in the Pd interlayer film is much smaller than the normal coherence or decay length in the junctions, indicating that the junctions are in the dirty-limit case.

### Conclusions

A method of fabricating trilayer Josephson junctions was successfully developed and is based on MgB<sub>2</sub> as the base electrode, with Pd as an interlayer and Nb as the counter-electrode. The junctions showed both  $dc$  and  $ac$  Josephson effect. The results indicate that it is possible to fabricate all-MgB<sub>2</sub> or MgB<sub>2</sub> as one electrode and another superconductor providing a second electrode based SNS and

SIS tunnel junctions with a wide range of interesting properties and useful applications.

#### Acknowledgements

The author is indebted to Dr. K. Ueda and Prof. M. Naito at NTT Basic Research Laboratories, NTT Corporation, Japan for providing the MgB<sub>2</sub> films and to Dr. A. Pavolotsky for his assistance when depositing the Pd and Nb films. The author is also indebted to his supervisors, particularly Prof. T. Claeson for the opportunity to work at the Microtechnology and Nanoscience Centre at Chalmers (MC2), Sweden. The work was supported by the Swedish Research Council (VR) and the Swedish Foundation for Strategic Research (SSF) through the OXIDE program.

#### References

- Chen K, Cui Y, Li Q, Zhuang CG, Liu ZK and Xi XX 2008 Study of MgB<sub>2</sub>/I/Pb tunnel junctions on MgO (211) substrates. *Appl. Phys. Lett.* 93: 125021-125023.
- Cybart SA, Chen K, Cui Y, Li Q, Xi XX and Dynes RC 2006 Planar MgB<sub>2</sub> Josephson junctions and series arrays via nanolithography and ion damage. *Appl. Phys. Lett.* 88: 125091-125093.
- Delin KA and Kleinsasser AW 1996 Stationary properties of high-critical-temperature proximity effect Josephson junctions. *Supercond. Sci. Technol.* 9: 227-234.
- Josephson BD 1962 Possible new effects in superconductive tunnelling. *Phys. Lett.* 1: 251-253.
- Kye JI, Lee HN, Park JD, Moon SH and Oh B 2003 Josephson effect in MgB<sub>2</sub>/Ag/MgB<sub>2</sub> step-edge junctions. *IEEE Trans. Appl. Supercond.* 13: 1075-1078.
- Mijatovic D, Brinkman A, Oomen I, Rijnders G, Hilgenkamp H, Rogalla H and Blank DHA 2002 Magnesium-diboride ramp-type Josephson junctions. *Appl. Phys. Lett.* 80: 2141-2143.
- Mijatovic D, Brinkman A, Oomen I, Veldhuis D, Rijnders G, Hilgenkamp H, Rogalla H and Blank DHA 2003 MgB<sub>2</sub> thin films and Josephson devices. *IEEE Trans. Appl. Supercond.* 13: 3245-3248.
- Mohseni M, Read P, Neven H, Boixo S, Denchev V, Babbush R, Fowler A, Smelyanskiy V and Martinis J 2017 Commercialize early quantum technologies. *Nature* 543: 171-174.
- Nagamatsu J, Nakagawa N, Muranaka T, Zenitani Y and Akimitsu J 2001 Superconductivity at 39 K in magnesium diboride. *Nature* 410: 63-64.
- Saito A, Kawakami A, Shimakage H, Terai H and Wang Z 2002 Josephson tunnelling properties in MgB<sub>2</sub>/AlN/NbN tunnel junctions. *J. Appl. Phys.* 92: 7369-7372.
- Schmid M and Menke H 2015 Josephson Effect. *Fortgeschrittenenpraktikum (FP)* 25: 1-10.
- Shapiro S 1963 Josephson currents in superconducting tunnelling: The effects of microwaves and other observations. *Physical Rev. Lett.* 11: 80-82.
- Shim H, Yoon KS, Moodera JS and Hong JP 2007 All-MgB<sub>2</sub> tunnel junctions with Al<sub>2</sub>O<sub>3</sub> or MgO tunnel barriers. *Appl. Phys. Lett.* 90: 2125091-2125093.
- Tsai JS 2010 Toward a superconducting quantum computer-Harnessing macroscopic quantum coherence. *Proc. Japan Acad. Ser. B* 86: 275-292.
- Ueda K and Naito M 2003a Tunnel junctions on as-grown superconducting MgB<sub>2</sub> thin films. *IEEE Trans. Appl. Supercond.* 13: 3249-3252.
- Ueda K and Naito M 2003b In situ growth of Superconducting MgB<sub>2</sub> thin films by molecular-beam epitaxy. *J. Appl. Phys.* 93: 2113-2120.
- Ueda K and Naito M 2004 Tunnel junctions on as-grown MgB<sub>2</sub> films. *Physica C* 408-410: 134-135.
- Ueda K and Naito M 2001 As-grown superconducting MgB<sub>2</sub> thin films prepared by molecular-beam epitaxy. *Appl. Phys. Lett.* 79: 2046-2048.
- Ueda K, Yamamoto H and Naito M 2002 Synthesis and photoemission study of as-grown superconducting MgB<sub>2</sub> thin films. *Physica C* 378-381: 225-228.
- Xi XX, Pogrebnyakov AV, Zeng XH, Redwing JM, Xu SY, Li Q, Liu Z-K, Lettieri J, Vaithyanathan V, Schlom DG, Christen HM, Zhai HY and Goyal A 2004 Progress in the deposition of MgB<sub>2</sub> thin films. *Supercond. Sci. Technol.* 17: S196-S201.